THE JOURNAL OF PHYSICAL CHEMISTRY C

Article

pubs.acs.org/JPCC

First-Principles Study of Biaxial Strain Effect on Hydrogen Adsorbed Mg (0001) Surface

Jia-Jun Tang,[†,‡,§] Xiao-Bao Yang,[†] Ming Chen,[†] Min Zhu,[‡,§] and Yu-Jun Zhao*[,†,‡]

[†]Department of Physics, South China University of Technology, Guangzhou 510640, P. R. China

[‡]Key Laboratory of Clean Energy Materials of Guangdong Higher Education Institute, South China University of Technology, Guangzhou 510640, P. R. China

[§]School of Materials Science and Engineering, South China University of Technology, Guangzhou 510640, P. R. China

ABSTRACT: We have studied hydrogen adsorption on the Mg(0001) surface under biaxial strain, using density-functional theory calculations. A phase diagram is obtained for an intuitive sense of how the strain and hydrogen chemical potential affect the structural stabilities of Mg−H system. It is found that the compressive (negative) strains facilitate the formation of the H−Mg−H trilayers, a precursor of the transition to magnesium hydride, due to the fact that the lattice constant of H−Mg−H trilayer is shorter than that of pure Mg. However, the magnesium hydride is more energetically favored with greater lattice constant caused by tensile (positive) strains which exceed +6%. During the hydrogenation, the H−Mg−H trilayer and MgH_2 bulk-like structures could be coexisting, where the strain is able to modulate their relative stabilities. These findings are helpful for the understanding of hydrogenation/dehydrogenation of the Mg−H system and could ultimately improve the design of Mg-based hydrogen storage materials.

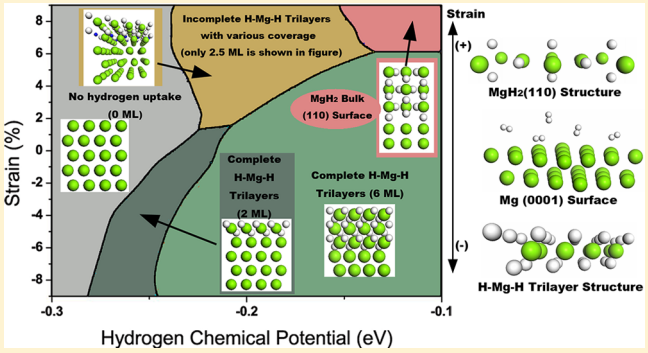

1. INTRODUCTION

The fossil fuels have been playing a vital role in human civilization. The world, however, faces a cruel fact that the fossil fuels will not take a long time to be run out of in the future.[1] Hydrogen energy, with high efficiency and environmental friendliness, is considered to be one of the most promising candidates of the clean energies and automotive applications.[2,3] There are three crucial steps for the hydrogen economy, i.e., production, storage, and utilization. It is a growing consensus that the hydrogen storage hits a bottleneck due to the lack of efficient hydrogen storage materials, which meet the ultimate gravimetric and volumetric targets (2.5 kWh/kg and 2.3 kWh/L) as well as proper kinetic performance set by DOE.[4]

Magnesium, which is fairly accessible at low cost, is a promising hydrogen carrying medium[5] for the onboard applications due to the high gravimetric hydrogen content, high volumetric density,[6] and the highest energy density,[7] i.e. 9 MJ/kg Mg. However, there are two main hurdles for MgH_2 for practical usage: (i) slow kinetics in the reaction of hydrogenation, which may account for surface oxidation of magnesium,[8] low dissociation rate of H_2 on magnesium surface,[9] and hydrogen penetration blocking induced by a surface magnesium hydride layer;[10,11] (ii) a high temperature of 350−400 °C and a high hydrogen pressure of more than 3 MPa are required for the hydrogenation and dehydrogenation reactions,[12] which is ascribed to its high thermodynamic stability.

To improve the efficiency of hydrogen storage, various methods have been applied to the design of Mg-based materials. Previous studies[13,14] showed that nanostructuring of magnesium materials provides rapid storage kinetics, especially in the hydrogen desorption process, since it lowered the activation energies of hydrogenation and dehydrogenation. Moreover, the nanostructuring-induced high surface area, both in Ti-catalyzed nanocrystalline MgH_2[13] and air-stable gas-barrier polymer matrix with Mg nanocrystals,[14] plays an important role in improvement of sorption kinetics. In addition, doping and alloying with other metals[15−18] have also improved the efficiency of hydrogen storage.

Strain, often introduced by the mismatched substrate during epitaxial growth of samples, may be a simple and controllable approach to modulate the efficiency of hydrogen storage materials. According to the model analysis,[19] the hydride process of a spherical metallic nanoparticle is found to be limited in the hydride phase by vacancy diffusion, which is influenced by lattice strain that impacts the gradient of hydrogen chemical potential and the vacancy diffusion coefficient in hydride shell. Experimentally, it has been reported that[20] the strain induced by high pressure torsion of Mg improves the hydrogen storage capacity drastically. Ye et al.[21] have found that the variation of hydrogen absorption and

Received: April 11, 2012
Revised: June 19, 2012
Published: June 25, 2012

desorption hydrogen pressure plateaus attributes to the strain created upon milling. Moreover, Higuchi et al.[22] reported that the improvement in the dehydriding properties in the multilayered Pd/Mg/Pd films is due to the elastic interaction, namely the strain effect, between metal layers. These reports implied that the strain effect could be helpful to the hydrogen storage properties of Mg or Mg-based materials.

In this paper, we have systematically investigated the biaxial strain effect on the Mg−H system by employing the calculations based on density-functional theory. Considering various Mg−H configurations, the stabilities of Mg−H compounds as a function of hydrogen chemical potential and the strain are determined. The theoretical method and model is mentioned in section 2, the results are described and discussed in section 3, and the paper is concluded in section 4.

2. METHODOLOGY

2.1. Computational Details. Our calculations are performed using Vienna Ab initio Simulation Package.[23−25] We use the exchange-correlation with generalized-gradient approximation (GGA)[26] and projector-augmented wave (PAW) potentials.[27] A 5 × 5 × 1 Monkhorst−Pack[28] k-point sampling is used for the Brillouin-zone integration, and the plane-wave cutoff energy was set to be 310 eV. The internal optimization is converged with the force on each atom to be less than 0.01 eV/Å. The energy convergence with respect to the k-points and cutoff energy has also been tested to be in the precision of ∼0.01 eV per cell.

We calculated the bulk Mg of hexagonal structure and found the optimized bulk lattice constant is a = 3.190 Å with the c/a value of 1.623, which is in good agreement with the experimental values[29] (a = 3.209 Å and c/a = 1.623) and previous theoretical results.[30−32] The Mg (0001) surface is modeled by a five-layer slab containing a 2 × 2 unit cell with a vacuum of 15 Å, and the lattice constant of the slab is optimized to be a = 3.134 Å. The difference of lattice constants is attributed to the small number of slab layers and is expected to disappear when the number of layers is large enough. For the hydrogen uptake, hydrogen atoms are placed evenly and gradually on both sides of the first three outermost Mg layers, where the two bottommost layers are fixed and the other layers are fully relaxed.

We have considered various adsorption configurations, as shown in Figure 1a−d. More specifically, there are four on-surface adsorption sites (top, bridge, hcp, and fcc, shown in Figure 1a) and three subsurface adsorption sites (octa, tetra1, and tetra2, as the superscripts of 1 and 2 indicate the first and the second outermost Mg layers shown in Figure 1b−d). The quantities of adsorbed hydrogen atoms are described by coverage θ, which indicates the number of adsorbed hydrogen monolayer. In our models, only the adsorption configurations with θ ranged from 0 to 6 ML are considered, where the hydrogen atoms are covering one by one on or below the magnesium layers from the first outermost to the third outermost. Note that two adsorption configurations on and below the second Mg layer, including the $f^1/t2^1 + h^2/o^2$ structure [shown in (g) and (h)] and the $f^1/t2^1 + f^2/t2^2$ one (not shown), are being considered.

2.2. Surface Thermodynamics. Adopting the formalism of *ab initio* atomistic thermodynamics, we compare the relative stabilities of surface structures under varied strains. The surface free energy is described as

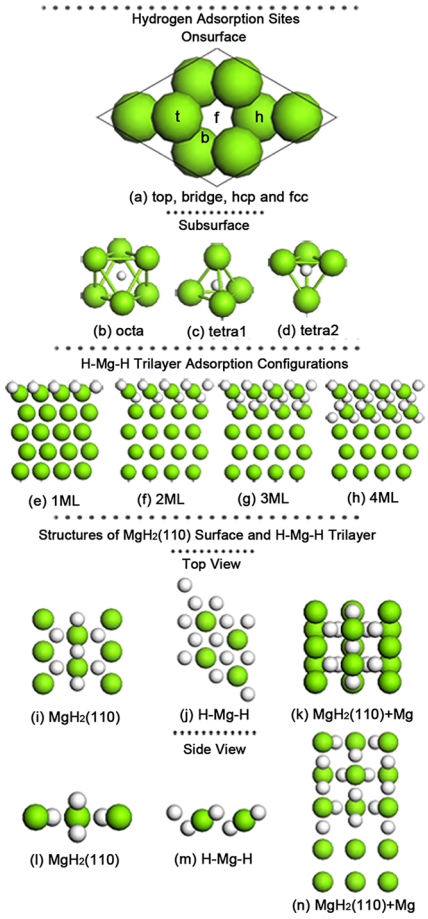

Figure 1. Calculation configurations used in this paper. (a−d) The hydrogen adsorption sites, on Mg(0001), of (a) on-surface top, bridge, hcp hollow, and fcc hollow (abbreviated as t, b, h, and f, respectively), (b) subsurface octa, (c) subsurface tetra1, and (d) subsurface tetra2. (e−h) The H−Mg−H trilayer adsorption configurations of (e) $\theta^1 = \theta^1_{on}$ = 1 ML (f^1 sites), (f) $\theta^1 = \theta^1_{on} + \theta^1_{sub}$ = 1 ML + 1 ML = 2 ML ($f^1/t2^1$), (g) $\theta_{TOT} = \theta^1 = \theta^1_{on}$ = 2 ML + 1 ML = 3 ML ($f^1/t2^1 + h^2$), (h) $\theta_{TOT} = \theta^1 = \theta^2$ = 2 ML + 2 ML = 4 ML ($f^1/t2^1 + h^2/o^2$). (i−n) (i) Top view and (l) side view of one layer of the $MgH_2(110)$ surface. (j) Top view and (m) side view of one H−Mg−H trilayer. (k) Top view and (n) side view of the structure of three $MgH_2(110)$ layers with two bottommost layers of magnesium atoms. The notations of configurations could simply be recognized by the symbol of abbreviations of adsorption sites (f, h, t, o) and the superscript, which represents the number of the topmost Mg layer. They are devided by the slash, which means the combination of the on-surface and subsurface adsorption sites. For example, $f^1/t2^1 + h^2/o^2$ means the on-surface and subsurface adsorption sites of the first and second topmost Mg layers are fcc, tetra2, hcp, and octa sites, respectively.

$$\gamma = \frac{1}{A}(G_{slab} - m\mu_{Mg} - x\mu_H) \quad (1)$$

where G_{slab} is the Gibbs free energy of the slab model used in our calculations, A is denoted as the in-plane surface area, and m and x are the numbers of the magnesium and adsorbed hydrogen atoms in the unit cell, respectively. The hydrogen chemical potential, μ_H, is tunable by the ambient environment to which the surface is exposed.

The magnesium chemical potential is assumed to be $\mu_{Mg} = (1/m)G_{PureMgSlab}$, where m is the number of magnesium atoms in the slab model of pure magnesium.

dx.doi.org/10.1021/jp303480c | J. Phys. Chem. C 2012, 116, 14943−14949

According to the literature,[33−37] the Gibbs free energies in eq 1 can be approximated as the total energies, E_{TOT}, calculated by the first-principles calculations, as the contributions from entropy and work done by pressure are negligible for the solid system. Consequently, G_{slab} and $G_{PureMgSlab}$ are replaced by $E_{Mg(0001)+xH}$ and $E_{Mg(0001)}$, respectively. The stable Mg−H compounds are obtained by determining the minima of surface energies under the sameμ_H, which depends on the ambient temperature T and pressure P.

To study the strain effect on the adsorption stability, we investigate various hydrogen adsorption configurations on the Mg slab under tensile and compressive strains. The lattice strain is given as follows: $\varepsilon_{xx} = (a - a_0)/a_0 \times 100\%$, where a (a_0) is the strained (unstrained) lattice constant Mg slab and ε_{xx} is in the range from −9% to 9%. A similar theoretical approach was previously adopted to study the biaxial strain effect of hexagonal wurtzite structures.[38] The average adsorption energy E_{ad} per hydrogen atom is calculated by

$$E_{ad} = \frac{1}{x}\left[E_{Mg(0001)+xH} - \left(E_{Mg(0001)} + \frac{x}{2}E_{H2}\right)\right] \quad (2)$$

where x is the number of the adsorbed hydrogen atoms in the system, and $E_{Mg(0001)+xH}$, $E_{Mg(0001)}$, and E_{H2} are the total energies of the optimized Mg−H adsorption system, the clean Mg slab, and H_2 in gas phase, respectively. The value of E_{ad} indicates the stability of hydrogen adsorption: a negative E_{ad} denotes that the hydrogen uptake is thermodynamically stable (exothermic), and the positive one represents that it is unstable (endothermic). Throughout the present work, both spin polarization and non-spin polarization are taken into account in the calculations, and the results show that the energy difference between them is negligible, which is in agreement with the result of Jiang et al.[31]

3. RESULTS AND DISCUSSION

Overall, various adsorption configurations mentioned above (shown in Figure 1) have been investigated under the strains ranged from −9% to +9%, and the total number of considered surface structures exceeds 350. We focus on the structure stability as a function of the strain and the hydrogen chemical potential, including an attempt of investigating the transition from the H−Mg−H trilayer to magnesium hydride bulk structure. In section 3.1, we present the phase diagram of structural stabilities. The phase transition of H−Mg−H trilayer to MgH_2 hydride is specified in section 3.2. The geometrical and electronic characteristics of H−Mg−H trilayer are discussed explicitly in section 3.3.

3.1. Phase Diagram of Mg−H System. The stable surface structures are determined as a function of strain and μ_H by the lowest surface free energy of all the calculated configurations at a given strain. The pressure and temperature range of interest in Figure 2 is determined by the hydrogen chemical potential, whose dependence on pressure and temperature was proposed by Reutal et al.[33] Test calculations show that H energetically favors the on-surface fcc site among seven potential adsorption sites on and below the outermost Mg layer of the slab at low coverage. Hydrogen atoms would be located at the subsurface tetra2 site after taking up all the four on-surface fcc sites, and the fcc/tetra2 configuration becomes the most energetically favored one (with the average adsorption energy of −0.26 eV) for θ = 2 ML, in line with the previous results.[31] As the hydrogen coverage increases, there are four typical adsorption

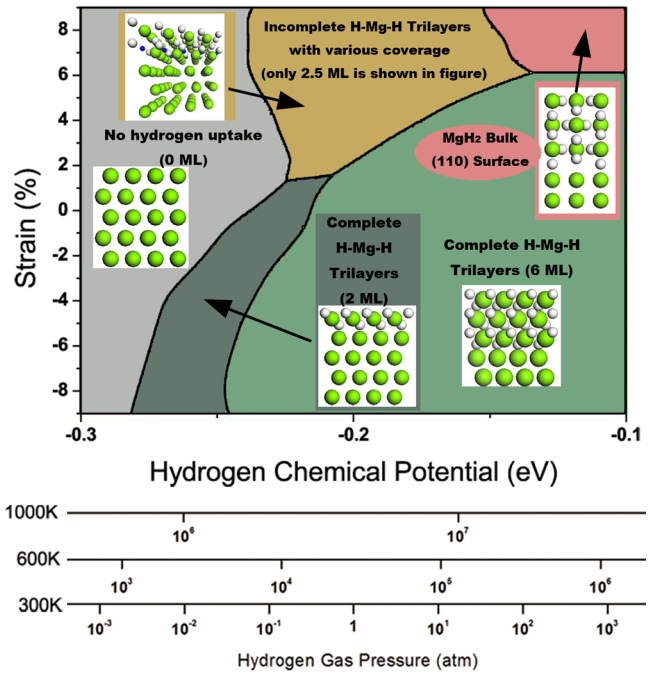

Figure 2. Structural stabilities phase diagram showing the principle surface structure regions of the hydrogen-adsorbed slab as a function of hydrogen chemical potential and biaxial lattice strain. Five insets are indicating the specific structures of the phase regions. The region of incomplete H−Mg−H trilayer includes four subregions, which are small in size and shown as the overall region in brown. Specifically, they are incomplete regions with θ = 1.5, 1.75, 2.25, and 2.5 ML. In the inset of 2.5 ML, the hydrogen atoms in blue represent the sites with no hydrogen atom adsorbed.

structures shown in Figure 1e−h, in which the H−Mg−H trilayers are regarded as a precursor of magnesium hydride[31] with the same chemical composition. We also consider the MgH_2(110) surface-like structures with the hydrogen coverage of 2, 4, and 6 ML, as shown in Figure 1k,n for θ = 6 ML.

The stable configurations with respect to the hydrogen chemical potentials and strains are summarized in a phase diagram as shown in Figure 2. There are three kinds of stable structures: the H−Mg−H trilayers, MgH_2(110) surface-like structures, and the intermediate structures (the incomplete trilayers). It is clear that H_2 uptakes are enhanced as μ_H increases. With the strains in the range between −9% and +2%, complete H−Mg−H trilayers are formed on the clean magnesium slab layer by layer, while the thermodynamically favorable surface structures are the incomplete H−Mg−H trilayers rather than those of the complete ones in the range from +2% to +9%. Thus, the system under compressive (negative) strains shows a preference for the formation of the H−Mg−H trilayers.

The calculated phase diagram (cf. Figure 2) also shows that the structure of the H−Mg−H trilayer is the most energetically favored within a wide range of strain and chemical potential. Thus, the formation of H−Mg−H trilayer is a highly competitive tendency during the hydrogen uptake. However, the structure of magnesium hydride will be more energetically favored when the hydrogen coverage reaches a critical value, which depends on the strain. MgH_2 is expected to be energetically favored at high H coverage, especially under tensile strain due to lattice expansion after H_2 uptake, while the incomplete trilayers could appear at relatively low H coverage.

dx.doi.org/10.1021/jp303480c | J. Phys. Chem. C 2012, 116, 14943−14949

It should be pointed out that, in our five-layer model, we keep the two bottommost layers fixed and consider the H_2 adsorption in the other three layers. Thus, the coverage of 6 ML corresponds to the maximum of H_2 uptake, which is the most stable for the high μ_H. It is found that the H−Mg−H trilayers with θ_{TOT} = 6 ML are more stable structures under strains ranged from −9% to +6%, while the phase transition into magnesium hydride structure would occur at the strain near +6% in our model. The compressive (negative) strains is found to facilitate the transition to the complete trilayers relatively more easily. The biaxial strain, therefore, imposed on the Mg−H system provides a tunable way for stabilizing the adsorption configuration.

In addition, in our model, the fact that the coverage of 6 ML corresponds to maximum of H_2 uptake cause the oversized region of complete trilayers of 6 ML in the phase diagram (cf. Figure 2). Also, it leads to the disappearance of the region of complete trilayer of 4 ML, which shows the similar competence on the adsorption energy with the complete trilayer of 6 ML. With a thicker model, the lattice of slab is expected to approach that of bulk and the regions of H−Mg−H trilayers with θ_{TOT} = 2n ML (n is positive interger) are expected to show up as the hydrogen chemical potential goes up. Nevertheless, the trend caused by the strain effect is still shown clearly despite of the limitedness of our five-layer model. With a thicker model, the phase transition into MgH_2 is thought to occur with less positive strains as the number of uptake hydrogen atom increases.

3.2. Stability of H−Mg−H Trilayers. We notice that the phase transition from θ_{TOT} = 0 region to a region where a complete H−Mg−H trilayer forms with θ_{TOT} = 2 ML seems to be abrupt for strain of −9% to +2% (cf. Figure 2). Our calculations show that the complete H−Mg−H trilayer is energetically more favored than other adsorption configurations. The local H−Mg−H trilayer, rather than the structures with hydrogen dispersed in the Mg film, tends to form when the coverage is less than 2 ML. Hence, the complete H−Mg−H trilayer with various monolayers dominates the phase diagram. In addition, the H−Mg−H trilayers are novel precursors, which possess a smaller lattice length compared to the Mg substrate, in contrast to the expectation of lattice expansion of the substrate due to H_2 uptake. The H−Mg−H trilayers are stable and the interactions between neighboring layers are weak. In the following sections, we would study the stability of the H−Mg−H trilayers on Mg(0001) surface according to the analysis of geometrical and electronic properties.

We have investigated the variations of hydrogen adsorption energies as a function of θ, as shown in Figure 3. The calculated adsorption energies are all with respect to the energy of H in its molecule as expressed in eq 2. The adsorption energy of complete trilayers corresponding to θ_{TOT} = 2 and 4 ML are more favored than those of the incomplete ones. The adsorption energies are also dependent on the adsorption configurations. The adsorption configuration prefers $f^1/t2^1$ + $f^2/t2^2$ to $f^1/t2^1$ + h^2/o^2 (cf. Figure 1), except for the situations of θ_{TOT} = 2.25 ML and θ_{TOT} = 2.5 ML with tiny differences of 0.01 eV. It indicates that the $f^1/t2^1$ + $f^2/t2^2$ configuration, when the coverage is in the range from 2 to 4 ML, is the most stable one among the studied adsorption configurations.According to the partial densities of states shown in the inset of Figure 3, it is found that the atomic orbital hybridization in H−Mg−H trailyer is dominated by bonding states consisting of Mg s and H s states. The hybridizations between Mg s and H s are strong

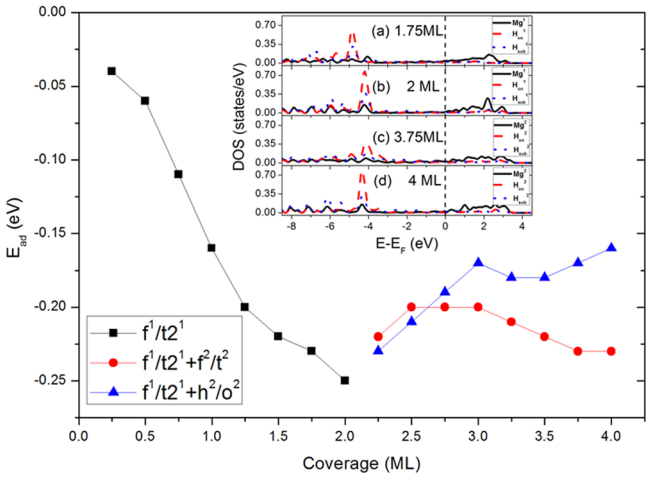

Figure 3. Adsorption energies of the system where the coverage range is between 0.25 and 4 ML at zero strain. In the coverage range from 2.25 to 4 ML, two adsorption configurations have been considered. The inset shows the partial densities of states for the hydrogen and Mg atoms of the same H−Mg−H trilayer ((a) and (b) in the first outermost one, (c) and (d) in the second outermost one) at zero strain.

in the complete trilayer (the peak sharpness), while the extents of the hybridizations are much weaker in the incomplete trilayers with θ_{TOT} = 1.75 ML and θ_{TOT} = 3.75 ML. Thus, the relative stabilities of the complete trilayers are attributed to the strong hybridization between Mg s and H s.

We further studied the structural symmetry of H−Mg−H trilayer, as the higher structural symmetry of the trilayer might strengthen the hybridization. The free H−Mg−H trilayer shows high symmetry at its lattice constant of 3.01 Å. More specifically, in a H−Mg−H bond, the bond lengths of Mg and both H_{on} and H_{sub} are 1.97 Å with a bond angle of 180°. It is, therefore, the straight-linear configuration where the electrostatic repulsion between the H atoms is screened by the middle Mg and a drastic system energy decrease occurs. Figure 4 shows the related structural variations of the system under strains. For a free H−Mg−H trilayer, shown in the inset of Figure 5, both the bonding state and the antibonding state are witnessing the peaks of strong hybridization between the Mg which stands in the middle and the two hydrogen atoms on both sides. Consequently, the configuration of high symmetry leads to a drastic system energy decrease and forms the ground state of H−Mg−H trilayer which is in high symmetry. The lattice preference of free H−Mg−H trilayer means that the pure Mg system with a smaller lattice constant of 3.01 Å, approximately −4% of the strain, tends to form the structure of H−Mg−H trilayer, especially when the hydrogen coverage is relatively low.

When the biaxial compressive strains are imposed on the a−b plane, the distance between two Mg on the same plane is shortened. This may cause the hurdle for the hydrogen diffusion along the [0001] direction. We estimate that the effect of squeezed Mg atoms does not influence the kinetic properties dramatically, and we here mainly focus on the thermodynamics problems. As shown above, the formation of H−Mg−H trilayer would shorten the distance between Mg atoms on the a−b plane. Thus, the H−Mg−H trilayers would become unstable when the tensile (positive) strains are imposed. In addition, the tensile strains on the Mg slab shorten the interlayer distance along the z direction. Figure 4a,b shows the variations of the interlayer spacing after the formations of H−Mg−H trilayers

dx.doi.org/10.1021/jp303480c | J. Phys. Chem. C 2012, 116, 14943−14949

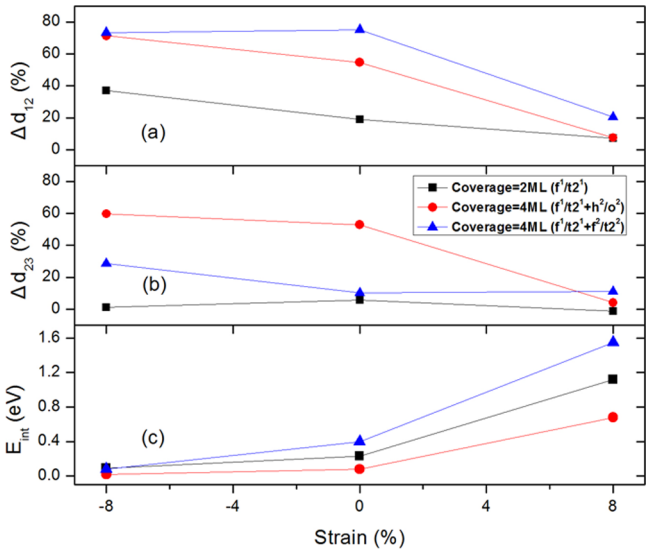

Figure 4. (a, b) Variations of spacing between the neighboring Mg layers in the configurations where the H−Mg−H trilayer(s) is (are) formed. (c) The interaction energies between the H−Mg−H trilayer(s) and the rest of Mg atoms. The variation of spacing Δd_{mn} is calculated by the following equation: $\Delta d_{mn} = (d_{mn} - d'_{mn})/d'_{mn} \times 100\%$, where d' and d and the subscripts of m and n mean the distances before and after structure optimization and the mth and nth outermost Mg layers, respectively. The interaction energies are calculated by the equation $E_{int} = E_{Trilayer(s)} + E_{RestofMgLayer(s)} - E_{Trilayer(s)/RestofMgLayer(s)}$.

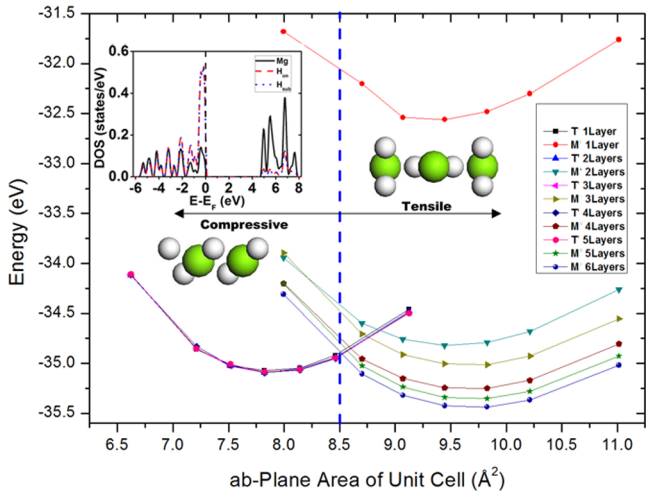

Figure 5. Comparisons of structural stabilities of multilayers of two structures. The blue line represents the *ab*-plane area of unit cell with lattice constant ($a = b = 3.134$ Å) of our slab model. The energies of each structure have been divided by the number of layers. The inset shows the partial densities of states for the hydrogen and Mg atoms of free H−Mg−H trilayer. T′ and M′ represent the structure of trilayers and $MgH_2(110)$ surface, respectively.

under strains. It is significantly enlarged with the compressive strains introduced while it does not change dramatically with the tensile strains introduced. We describe the coupling by the interaction energies (E_{int}) between the trilayers and the rest of the magnesium atoms underneath, as shown in Figure 4c. The coupling is significantly weakened at negative strains with the E_{int} of 0.1 eV, while the E_{int} is much greater at tensile strains. The stronger coupling indicates that the trilayers can not be independently stable under large tensile strains, which confirms the rationality of the existence of the incomplete trilayer(s) in the phase diagram. As the tensile strain increases, the stabilities of H−Mg−H trilayers decrease and the coupling between interlayers increases, leading to the transitions from the complete H−Mg−H trilayers to the incomplete ones and the MgH_2 bulk structures finally.

3.3. Phase Transition from H−Mg−H Trilayers to MgH_2. According to the phase diagram, there will be either a stacking of the H−Mg−H trilayers or a phase transition to MgH_2 bulk structure, depending on the biaxial strain, as the hydrogen coverage keeps increasing. We take in account both the H−Mg−H trilayer and the MgH_2 (110) surface structures, investigating the stability dependence on both the strain and the number of layers (shown in Figure 5). It is manifested that the total energy decreases remarkably with the increasing number of layers of the $MgH_2(110)$ surface structure, while the energies of the H−Mg−H trilayers are insensitive to the number of trilayers. The interaction between the trilayers is clearly weak, since the single H−Mg−H trilayer is stable with a large energy difference over 4 eV (shown in the inset of Figure 5). When the number of layers is four or more, the $MgH_2(110)$ surface structure is more energetically favored. The structure of H−Mg−H trilayer acts like a precursor, and the transition will occur as the coverage increases. The favored lattice constants of the H−Mg−H trilayer and the structure of single layer of MgH_2 (110) surface are found to be 3.01 and 3.45 Å, respectively. Though the interface of MgH_2 and H−Mg−H trilayer is complicated, the negative strain is expected to enhance the stability of the H−Mg−H trilayer, and MgH_2 (110) surface will be energetically favored at the positive strain since the lattice constant of Mg film is 3.134 Å. It can be inferred that, during the hydrogenation, the structure of H−Mg−H trilayer shows big energetic advantages at the beginning and has a great impact at the initial stage of hydrogenation while the structure of $MgH_2(110)$ surface is absolutely more favored as θ reaches a critical value. The reason is that the drastic energy decrease would be induced by the saturation of dangling bonds in the structure of $MgH_2(110)$ surface as the number of hydrogen adsorbed Mg layers keeps increasing. Therefore, the bulk-like structure tends to form as the hydrogen atoms penetrate into the Mg material. Of note, the lattice constant we defined here is based on an assumption of the hexagonal unit cell of Mg *ab*-plane. The included angle between *a*- and *b*-axes of H−Mg−H trilayer is found to be 120° while the one of $MgH_2(110)$ is 129°19′, suggesting that the Mg atoms on $MgH_2(110)$ surface unit cell is as-hexagonal. The area of the *ab*-plane of the unit cell, therefore, is adopted in Figure 5 to describe the strain effect more intuitionally rather than the lattice constants themselves. It is known that the high temperature is always required for the Mg−MgH_2 phase transition.[39] The lattice constant preference of the single layer of MgH_2 (110) surface may illustrate us a possible approach of promoting the Mg−MgH_2 phase transition by imposing a positive strain.

According to our study, the metal−hydride phase transition resulted from the competition between the H−Mg−H trilayer and MgH_2. That is, when the hydrogenation starts (θ is small), the system without strain prefers to the formation of H−Mg−H trilayer(s). Subsequently, the formation of H−Mg−H trilayer(s), which has a smaller lattice constant, will induce the compressive (negative) strains and facilitate the formation of more H−Mg−H trilayers. As θ increases, the MgH_2 structures would be energetically more favorable, and the phase transition occurs. Meanwhile, the tensile (positive)

dx.doi.org/10.1021/jp303480c | J. Phys. Chem. C 2012, 116, 14943−14949

strains will be induced and the MgH_2 structure is further stabilized as it has a greater lattice constant. Thus, the compressive (negative) strain is important at the initial stage of hydrogen adsorption on Mg metal, leading to a more easily formed H−Mg−H trilayer structure.

It is concluded that the strain effect is important for the hydrogenation process because it can lead the hydrogen adsorbed system to different stable structures. Namely, the strains can be utilized as a tool to tune the hydrogenation process. Although MgH_2 is energetically favored at the positive strain region in the phase diagram, where all the strains are with respect to the lattice constant of pure Mg slab (3.134 Å), a negative (compressive) strain with respect to the lattice of MgH_2 is required to destabilize it and thus facilities the dehydrogenation process.

Note that the phase transition from trilayer to hydride is complicated, which concerns not only the energetic stabilities of structures but also interface matching. Experimentally, Kelekar et al.[40] have found that the MgH_2(110) surface could form epitaxially on Mg(001) surface, which shares similar arrangements of Mg atoms with MgH_2(110) surface. For simplicity, the interface matching here is based on similar arrangements of Mg atoms of H−Mg−H trilayer and MgH_2 (110) surface for a preliminary study. Nevertheless, the trend of the phase transition from H−Mg−H trilayer to MgH_2 with respect to H chemical potential and strain (cf. Figure 2) are reasonable based on our discussions.

In fact, there are some recent experimental observations and theoretical reports supporting our discussions above. Baldi et al.[41] indicated experimentally that the clamping effect, which can be regarded to the compressive (tensile) effect in our work, results in a higher MgH_2 formation enthalpy and is the hurdle for the metal−hydride formation of H−Mg−H trilayers precursor. From theoretical prospective, Jiang et al.[31] showed that the sequence of phase transition during hydrogen uptake was: five pure magnesium layers → one H−Mg−H trilayer and four pure magnesium layers→ two H−Mg−H trilayers and three pure magnesium layers → transition to magnesium hydride. It is mainly in accordance with the result shown in our phase diagram. Jiang et al.[31] forecast the trilayer−hydride transition happens as the coverage reaches to 6 ML in the way of stacking the MgH_2(110) surfaces freely, which leads to a lower formation of energy. The model we used (see Figure 1k,n) is built based on the lattice of pure Mg(0001) surface, in order to stimulate the authentic hydrogen uptake process. Consequently, the lattice misfit of the bottommost layers of pure Mg and the layers of MgH_2(110) surfaces results in a high total energy for the MgH_2 phase.

4. CONCLUSION

In summary, we have investigated the biaxial strain effects on the magnesium hydrogen storage material. According to the phase diagram and the analysis geometrical and electronic properties, we demonstrated that the compressive (negative) strains benefit the hydrogenation to form H−Mg−H trilayers precursor at the initial stage with relatively small number of layers. With further hydrogen uptake, bulk MgH_2 is energetically favored, especially under tensile (positive) strain with respect to the lattice constant of Mg slab. We found that the stability of H−Mg−H trilayers precursor, which is vital at the initial stage of hydrogen adsorption, can be modulated by the biaxial strain effectively. Negative (compressive) strains can facilitate the hydrogenation process for Mg system at the initial stage. Negative strains (with respect to the lattice of MgH_2, not the reference of Mg slab as adopted in Figure 2) also promote the dehydrogenation of the MgH_2 systems. We propose that the biaxial strain tuned hydrogenation/dehydrogenation could provide a practical approach for promoting the efficiency of the Mg−H system.

AUTHOR INFORMATION

Corresponding Author

*Tel +86-20-87110426; fax +86-20-87112837; e-mail zhaoyj@scut.edu.cn.

Notes

The authors declare no competing financial interest.

ACKNOWLEDGMENTS

This work was supported by MOST under project 2010CB631302, NSFC (Grant 11104080), the Fundamental Research Funds for the Central Universities (Grant 2011ZM0090), and Guangdong Natural Science Foundation (S2011040005430). The computing resources from the HPC Lab, Shenzhen Institute of Advanced Technology, Chinese Academy of Sciences (CAS), and from ScGrid of the Supercomputing Center, Computer Network Information Center of CAS, are gratefully acknowledged.

REFERENCES

(1) Jena, P. *J. Phys. Chem. Lett.* **2011**, *2*, 206−211.
(2) Schlapbach, L.; Zuttel, A. *Nature* **2001**, *414*, 353−358.
(3) Schwarz, R. B. *MRS Bull.* **1999**, *24*, 40−44.
(4) US Department of Energy. Targets for Onboard Hydrogen Storage Systems for Light-Duty Vehicles; http://www1.eere.energy.gov/hydrogenandfuelcells/mypp/pdfs/storage.pdf (accessed May 2009), pp 3.3−8.
(5) Sakintuna, B.; Lamari-Darkrim, F.; Hirscher, M. *Int. J. Hydrogen Energy* **2007**, *32*, 1121−1140.
(6) Selvam, P.; Viswanathan, B.; Swamy, C. S.; Sprinivasan, V. *Int. J. Hydrogen Energy* **1986**, *11*, 169−192.
(7) Fukai, Y. *The Metal-Hydrogen System: Basic Bulk Properties*, 2nd ed.; Springer Series in Materials Science; Springer: Berlin, 2005; p 497.
(8) Zaluska, A.; Zaluski, L.; Strom-Olsen, J. O. *J. Alloys Compd.* **1999**, *288*, 217−225.
(9) Schlapbach, L.; Shaltiel, D.; Oelhafen, P. *Mater. Res. Bull.* **1979**, *14*, 1235−12461246.
(10) Luz, Z.; Genossar, J.; Rudman, P. S. *J. Less-Common Met.* **1980**, *73*, 113−118118.
(11) Krozer, A.; Kasemo, B. *J. Phys.: Condens. Matter* **1989**, *1*, 1533−15381538.
(12) Mushnikov, N. V.; Ermakov, A. E.; Uimin, M. A.; Gaviko, V. S.; Terent'ev, P. B.; Skripov, A. V.; Tankeev, A. P.; Solonin, A. V.; Buzlukov, A. L. *Phys. Met. Metallogr.* **2006**, *102*, 421−431.
(13) Shao, H. F.; Schuth, M.; Weidenthaler, F. *Nanotechnology* **2011**, *22*, 235401.
(14) Jeon, K. J.; Moon, H. R.; Ruminski, A. M.; Jiang, B.; Kisielowski, C.; Bardhan, R.; Urban, J. J. *Nat. Mater.* **2011**, *10*, 286−290.
(15) Chen, M.; Yang, X. B.; Cui, J.; Tang, J. J.; Gan, L. Y.; Zhu, M.; Zhao, Y. J. *Int. J. Hydrogen Energy* **2012**, *37*, 309−317.
(16) Berlouis, L. E. A.; Cabrera, E.; Hall-Barientos, E.; Hall, P. J.; Dodd, S. B.; Morris, S.; Imam, M. A. *J. Mater. Res.* **2001**, *16*, 45−57.
(17) Andreasen, A. *Int. J. Hydrogen Energy* **2008**, *33*, 7489−7497.
(18) Crivello, J. C.; Nobuki, T.; Kuji, T. *Int. J. Hydrogen Energy* **2009**, *34*, 1937−1943.
(19) Zhdanov, V. P. *Chem. Phys. Lett.* **2010**, *492*, 77−81.
(20) Edalati, K.; Yamamoto, A.; Horita, Z.; Ishihara, T. *Scr. Mater.* **2011**, *64*, 880−883.
(21) Ye, S. Y.; Chan, S. L. I.; Ouyang, L. Z.; Zhu, M. *J. Alloys Compd.* **2010**, *504*, 493−497.

(22) Fujii, H.; Higuchi, K.; Yamamoto, K.; Kajioka, H.; Orimo, S.; Toiyama, K. *Mater. Trans.* **2002**, *43*, 2721−2727.
(23) Kresse, G.; Hafner, J. *Phys. Rev. B* **1993**, *47*, 558−561.
(24) Kresse, G.; Furthmuller, J. *Comput. Mater. Sci.* **1996**, *6*, 15−50.
(25) Kresse, G.; Furthmuller, J. *Phys. Rev. B* **1996**, *54*, 11169−11186.
(26) Perdew, J. P.; Burke, K.; Ernzerhof, M. *Phys. Rev. Lett.* **1996**, *77*, 3865−3868.
(27) Kresse, G.; Joubert, D. *Phys. Rev. B* **1999**, *59*, 1758−1775.
(28) Monkhorst, H. J.; Pack, J. D. *Phys. Rev. B* **1976**, *13*, 5188−5192.
(29) Kittle, C. *Introduction to Solid State Physics*, 8th ed.; Wiley: New York, 2005.
(30) Du, A. J.; Smith, S. C.; Yao, X. D.; Lu, G. Q. *J. Phys. Chem. B* **2005**, *109*, 18037−18041.
(31) Jiang, T.; Sun, L. X.; Li, W. X. *Phys. Rev. B* **2010**, *81*, 035416.
(32) Vegge, T. *Phys. Rev. B* **2004**, *70*, 035412.
(33) Reuter, K.; Scheffler, M. *Phys. Rev. B* **2001**, *65*, 035406.
(34) Reuter, K.; Scheffler, M. *Phys. Rev. Lett.* **2003**, *90*, 046103.
(35) Meyer, B.; Marx, D. *Phys. Rev. B* **2003**, *67*, 035403.
(36) Kresse, G.; Dulub, O.; Diebold, U. *Phys. Rev. B* **2003**, *68*, 245409.
(37) Warschkow, O.; Chuasiripattana, K.; Lyle, M. J.; Delley, B.; Stampfl, C. *Phys. Rev. B* **2011**, *84*, 125311.
(38) Wagner, J. M.; Bechstedt, F. *Phys. Rev. B* **2002**, *66*, 115202.
(39) Wu, C. Z.; Wang, P.; Yao, X. D.; Liu, C.; Chen, D. M.; Lu, G. Q.; Cheng, H. M. *J. Phys. Chem. B* **2005**, *109*, 22217−22221.
(40) Kelekar, R.; Giffard, H.; Kelly, S. T.; Clemens, B. M. *J. Appl. Phys.* **2007**, *101*, 114311.
(41) Baldi, A.; Gonzalez-Silveira, M.; Palmisano, V.; Dam, B.; Griessen, R. *Phys. Rev. Lett.* **2009**, *102*, 226102.